Noise-induced resistance broadening in resistive switching memory (RRAM) - Part I: Intrinsic cell behavior

Stefano Ambrogio, *Student Member, IEEE*, Simone Balatti, *Student Member, IEEE*, Vincent McCaffrey, Daniel Wang, Daniele Ielmini, *Senior Member, IEEE*

I. Introduction

Resistive switching memory (RRAM) [1] and conductive bridge RAM (CBRAM) [2]–[4] are based on the voltage-controlled formation and dissolution of a conductive filament (CF) across an insulating layer, usually a metal oxide. The device is in a low resistance state (LRS) when the CF connects the top and bottom electrodes, otherwise the device is in a high resistance state (HRS). RRAM and CBRAM (RRAM will be used to indicate both technologies in the following) have become promising technologies for future nonvolatile memory applications, due to their fast switching, low power consumption and good endurance [5]. Among the open challenges for RRAM reliability, stochastic switching variability [6] and low-frequency current fluctuations such as $1/f$ noise [7]–[9] and random telegraph noise (RTN) [10]–[17] need to be addressed and controlled. While statistical fluctuation of set/reset processes, i.e. program noise and switching variability, can be addressed by program/verify techniques, read noise can hardly be predicted and corrected by system engineering, e.g., program/verify loops. Therefore, read noise represents the primary reliability concern for RRAM.

RRAM noise arises due to atomistic fluctuations of defects along the CF in LRS and the localized conductive path in HRS. It was shown that the relative amplitude of LRS noise increases with resistance, as a result of size-dependent depletion within the CF [13]. The reliability impact of RTN can be reduced in part by reading at relatively high voltage, where the noise amplitude decreases and the fluctuation-frequency increases due to thermally-activated kinetics of defect fluctuation [11]. However, a proper control of noise and noise-induced level broadening is still a major challenge for RRAM [7].

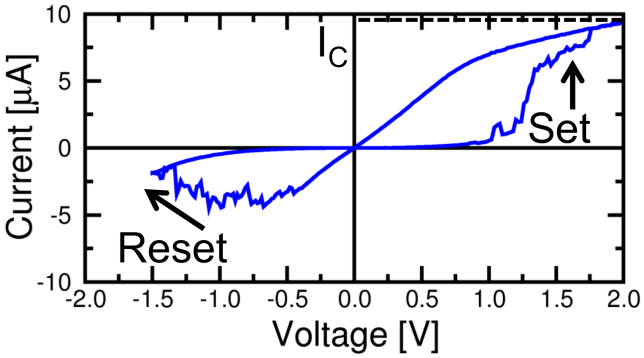

Fig. 1. Measured I-V curve for a RRAM device in a 1T1R structure with a compliance current I_C = 9 μA. The set and reset transitions appear for positive and negative voltages respectively.

This work addresses the impact of low frequency fluctuations in intrinsic RRAM devices. We find that resistance broadening with time is due to $1/f$ noise and RTN, and derive an analytical formula to predict the resistance spread as a function of time. The resistance-dependence of $1/f$ noise in LRS and HRS is then studied and explained in terms of multiple-defect fluctuations by finite element calculations.

A preliminary study on noise-induced broadening of RRAM resistance was reported in [7]. Here we extend the analysis of [7] by addressing the resistance-dependence of noise in LRS and HRS by experiments and simulations. The statistics of noise causing array distribution broadening will be addressed in the companion paper [18].

II. RRAM devices and characteristics

We performed experiments on RRAM devices with a one-transistor/one-resistor (1T1R) structure. The RRAM element consisted of a stack of a Cu-containing amorphous alloy as an active top electrode, a metal oxide layer of 6 nm thickness, and an inert metal bottom electrode [7]. RRAM with Cu-containing top electrode is believed to rely on the migration of Cu ions for set and reset processes. This type of devices is sometimes

S. Ambrogio, S. Balatti and D. Ielmini are with the Dipartimento di Elettronica, Informazione e Bioingegneria and Italian Universities Nanoelectronics Team (IU.NET), Politecnico di Milano, piazza L. da Vinci 32, 20133 Milano, Italy. E-mail: daniele.ielmini@polimi.it. V. McCaffrey and D. Wang are with Adesto Technologies, Sunnyvale, California, USA.

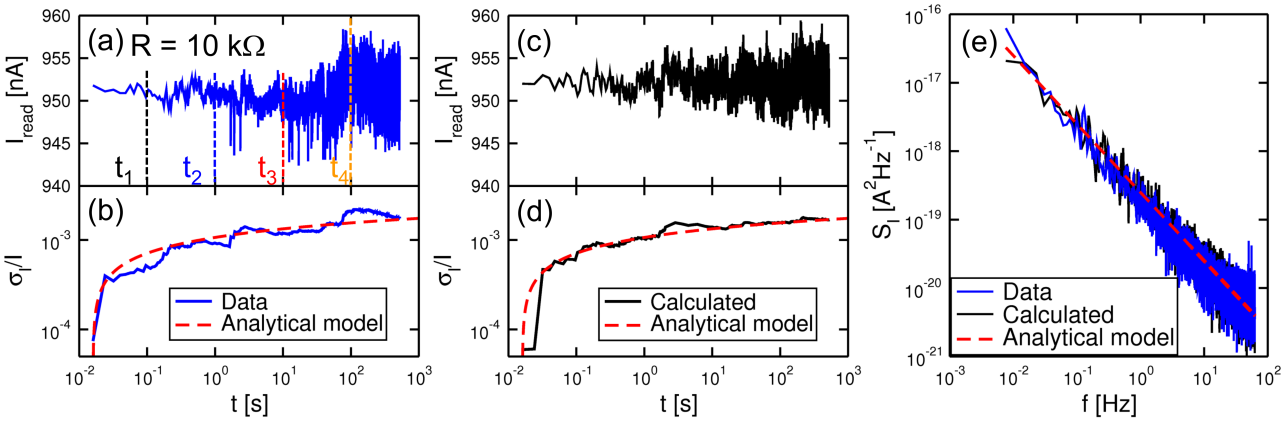

Fig. 2. Measured read current as a function of time for LRS with R = 10 kΩ (a), its corresponding relative standard deviation σ_I/I (b), calculated current as a function of time (c) and its relative standard deviation (d), and PSD of experimental and calculated noise (e). The PSD indicates a $1/f$ behavior of noise in the device. The results of the analytical model are also reported in (b,d,e), showing a good agreement with experimental and numerical results.

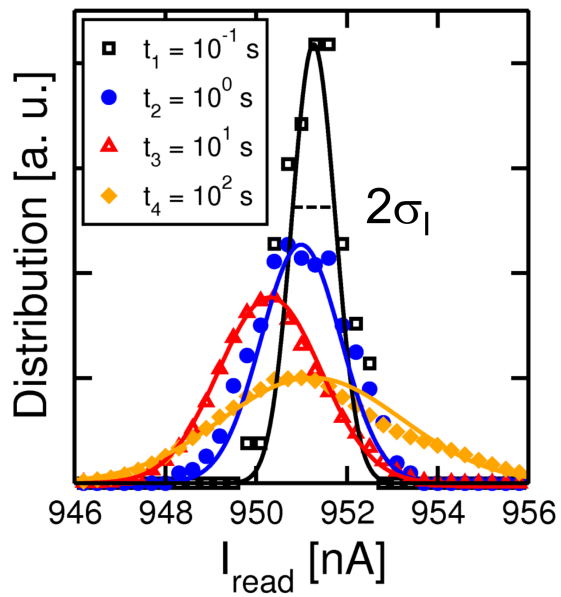

Fig. 3. Measured I_{read} distributions for increasing times $t_1 = 10^{-1}$ s, $t_2 = 1$ s, $t_3 = 10^1$ s and $t_4 = 10^2$ s shown in Fig. 2a. The gaussian fits are also shown with normalized areas. The standard deviation σ increases for increasing time due to $1/f$ noise as also shown in Fig. 2b.

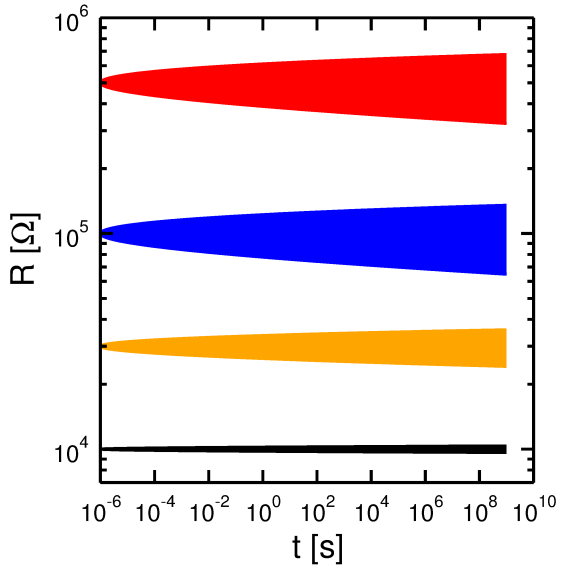

Fig. 4. Calculated 6σ broadening of resistance levels with time due to $1/f$ noise, according to Eq. (2).

referred to as conductive bridge RAM (CBRAM) [4], [19], although the name RRAM will be used here for the sake of generality. Two different RRAM stacks were used, namely stacks A and B, differing by the metal oxide although showing similar noise behavior. All measurements have been performed on stack A, except where noted.

Fig. 1 shows the measured I-V curve where the set transition from HRS to LRS occurs by applying a positive voltage to the top electrode, leading to the formation or connection of a conductive filament (CF) across the oxide layer. The current increase is limited by the select transistor to a compliance current I_C which is about 9 μA in Fig. 1. Reset transition from LRS to HRS is instead obtained by a negative voltage inducing partial dissolution of the CF by ion migration toward the top electrode [20], [21].

III. $1/f$ NOISE BEHAVIOR AND MODELING

Fig. 2a shows the measured read current I_{read} obtained for a 10 kΩ set state with a read voltage V_{read} = 10 mV. Current fluctuations are due to $1/f$ noise, which is evidenced by the power spectral density (PSD) S_I in Fig. 2e, revealing a clear -1 slope. All measurements were performed in the steady state of noise fluctuations, namely, the PSD did not depend on the time of the measurement of I_{read}. We neglected the noise contribution of the transistor which is much smaller compared to the resistive switching device noise in the 1T1R structure. In fact, we observed that the measured noise characteristics changes from cycle to cycle, e.g., from $1/f$ noise to RTN, which clearly indicates that the RRAM element dominates the device noise characteristic. To understand the impact of $1/f$ noise on cell readout, we extracted the I_{read} distributions at

increasing times t_1 = 0.1 s, t_2 = 1 s, t_3 = 10 s and t_4 = 100 s, as indicated in Fig. 2a. Here, the distribution at a generic time t_i contains all I_{read} samples collected before t_i with a sampling frequency of 125 Hz. The results normalized by the overall area of the distribution are reported in Fig. 3 together with their respective gaussian fits. The standard deviation σ_I of I_{read} increases with time due to the increasing contribution of fluctuations at low frequency, which are characterized by a higher PSD. Fig. 2b shows the relative standard deviation σ_I/I, where I is the median value of I_{read} from zero to time t. Results in the figure confirm that σ_I/I increases with time due to the increasing noise contributions at low frequency.

To better understand the impact of $1/f$ noise on resistance broadening, we simulated $1/f$ noise in I_{read} by a numerical Monte Carlo model. Fig. 2c shows the calculated I_{read} as a function of time, while Fig. 2e shows the corresponding PSD demonstrating $1/f$ dependence of noise in the frequency domain. Fig. 2d shows the corresponding relative spread σ_I/I as a function of time, which accounts for the experimental data in Fig 2b. These results support our interpretation of the distribution broadening with time, which affects the resistance distribution of RRAM.

A. Analytical modeling

We developed an analytical model to predict the time-dependent broadening of I_{read} distributions. The variance ${\sigma_I}^2$ can be calculated by integrating the S_I spectrum from a minimum frequency f_{min} to a maximum frequency f_{max} [22] according to:

$$ {\sigma_I}^2 = \int_{f_{min}}^{f_{max}} S_I df, \tag{1} $$

where $f_{min} = t^{-1}$, $f_{max} = (2t_s)^{-1}$ and t_s is the sampling time, of 8 ms in Fig. 2. By substituting S_I=A/f in Eq. (1), where the parameter A is the PSD S_I at a frequency f = 1 Hz, the relative ratio σ_I/I can be analytically obtained by:

$$ \frac{\sigma_I}{I} = \frac{\sqrt{A ln(f_{max} t)}}{I}. \tag{2} $$

The calculated results are plotted in Fig. 2b and d, showing a good agreement with data and numerical calculations. The corresponding S_I is reported in Fig. 2e. From Eqs. (1) and (2), the broadening of I_{read} distribution with time can be understood by the integration range extending to decreasing f_{min}, where the PSD largely increases due to the $1/f$ dependence of the PSD. Eq. (2) provides a useful tool for easily evaluating the broadening of a current level (or, equivalently, a resistance level due to the relationship $\sigma_I/I = \sigma_R/R$) with time. For instance, the analytical model straightforwardly allows for a rapid feasibility study of multilevel cell operation as shown in Fig. 4. Here, four different resistance levels R_1 = 10 kΩ, R_2 = 30 kΩ, R_3 = 100 kΩ, R_4 = 500 kΩ are considered as an example, together with their six-σ broadening with time according to Eq. (2), where $A_{10k\Omega}$ = 10^{-18} A^2, $A_{30k\Omega}$ = 3.3x10^{-18} A^2, $A_{100k\Omega}$ = 10^{-18} A^2 and $A_{500k\Omega}$ = 4x10^{-20} A^2 were assumed. Note that the 100 kΩ and 500 kΩ resistance levels in Fig. 4 display a similar spread on the log-scale, which corresponds to similar σ_R/R. The extension to 10 years reveals feasibility of multilevel cell operation. Note that calculations were performed considering the median values of noise and not the entire noise distribution. In fact, high noise cells lead to the failure of multilevel cell due to excessive fluctuations.

IV. Analytical Model of RTN

RTN was also studied similar to $1/f$ noise. Fig. 5a shows the measured I_{read} as a function of time, for a RRAM device in the LRS with a resistance R = 15 kΩ measured at V_{read} = 10 mV. Note that we used the same experimental conditions for measuring both $1/f$ noise (Fig. 2) and RTN (Fig. 5). RTN and $1/f$ noise can appear on the same device for different cycles, depending on the number of defects and on the impact of the charge fluctuation on the CF current. The measured current clearly displays RTN with a relative amplitude of almost a factor 2. The extracted σ_I/I ratio is reported in Fig. 5b. Interestingly, σ_I/I is initially negligible, until the first current step occurs at 0.7 s, at which point σ_I/I sharply increases due to the increased spread caused

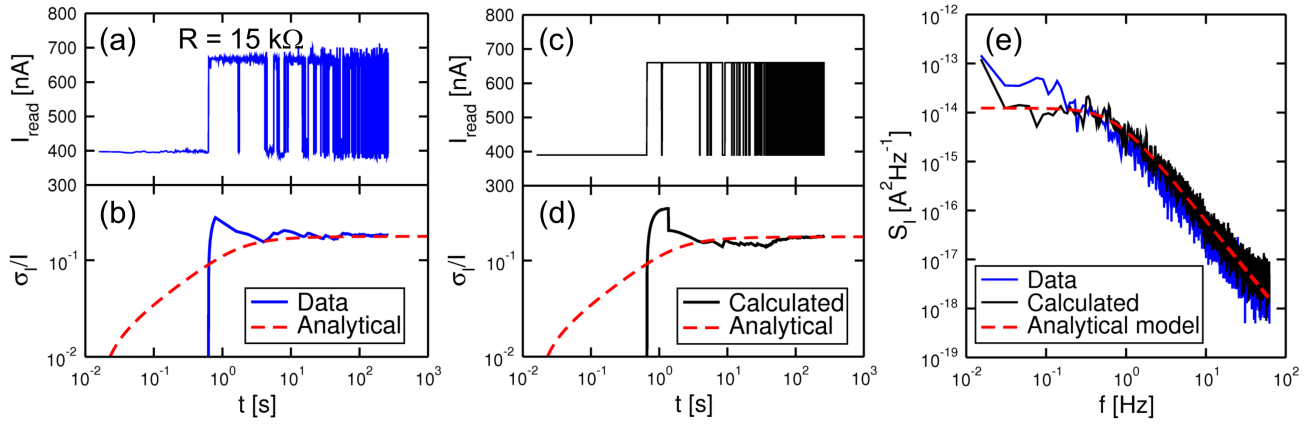

Fig. 5. Measured read current as a function of time for LRS with R = 15 kΩ (a), its corresponding relative standard deviation σ_I/I (b), calculated current as a function of time (c) and its relative standard deviation (d), and PSD of experimental and calculated noise (e). The PSD indicates an RTN behavior of noise in the device. The results of the analytical model are also reported in (b,d,e), showing a good agreement with experimental and numerical results.

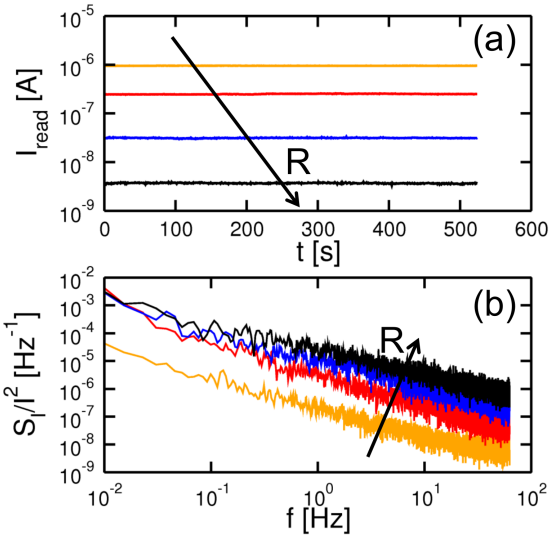

Fig. 6. Measured I_{read} as a function of time (a) for different resistances from 10 kΩ to 2.6 MΩ and corresponding PSD (b). Data show a $1/f$ behavior in the frequency domain, where PSD increases with R, then saturates at relatively high R.

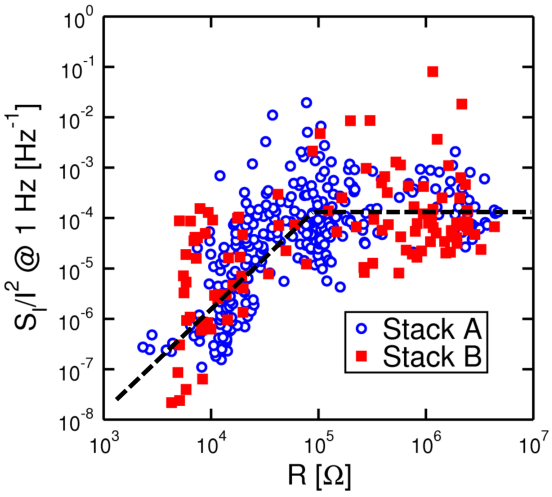

Fig. 7. Measured S_I/I^2 at 1 Hz as a function of R for stacks A and B. The regimes below and above R = 80 kΩ reveal the transition from partial to full depletion in the CF. Data from RRAM with stack A and B do not show significant difference.

by the change in the current level. In contrast to the $1/f$ case, the σ_I/I ratio does not continuously increase, rather it saturates to a constant value of about 0.2 due to the presence of only 2 levels in the current distribution. From a frequency-domain perspective, the saturation of σ_I/I at long times can be understood by the saturated PSD of the Lorentzian shape of RTN at decreasing f_{min}, hence increasing times.

To derive an analytical formula for σ_I/I, we first introduce the characteristic time constant τ_P of RTN given by:

$$\tau_P = \frac{\tau_{on}\tau_{off}}{\tau_{on}+\tau_{off}}, \tag{3}$$

where τ_{on} and τ_{off} are the average times for the current to switch from high to low value, and from low to high value, respectively. From Eq. (3), τ_P defines the pole of the current fluctuation. It can be shown that S_I is a Lorentzian function given by [23]:

$$S_I = 4\Delta I^2 \frac{1}{\tau_{on}+\tau_{off}} \frac{\tau_P^2}{1+(2\pi f)^2\tau_P^2}, \tag{4}$$

where ΔI represents the difference between the 2 current levels in the RTN. Following the same procedure adopted for $1/f$ noise in Eq. (1), the variance σ_I^2 is obtained by integrating S_I from f_{min} to f_{max} thus leading to:

$$\sigma_I^2 = \frac{2\Delta I^2\tau_P}{\pi(\tau_{on}+\tau_{off})}(atan(2\pi\tau_P f_{max}) - atan(\frac{2\pi\tau_P}{t})). \tag{5}$$

Eq. (5) can be simplified as:

$$\frac{\sigma_I}{I} = \frac{\sqrt{\alpha - \beta atan(\frac{2\pi\tau_P}{t})}}{I}, \tag{6}$$

where α is given by:

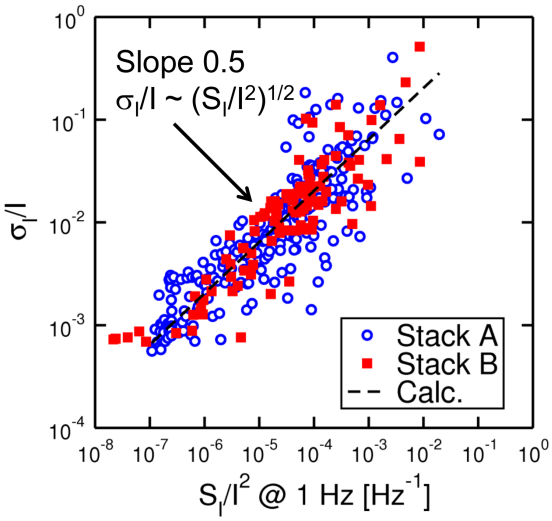

Fig. 8. Scatter plot of σ_I/I at 520 s as a function of S_I/I^2 at 1 Hz. The slope = 0.5 is consistent with the analytical model of Eq. (2). Data from RRAM with stack A and B do not show significant difference.

$$\alpha = \frac{2\Delta I^2\tau_P}{\pi(\tau_{on}+\tau_{off})} atan(2\pi\tau_P f_{max}), \tag{7}$$

and β is given by:

$$\beta = \frac{2\Delta I^2\tau_P}{\pi(\tau_{on}+\tau_{off})}. \tag{8}$$

Calculation results from the analytical model are shown in Fig. 5b, showing an initial increase corresponding to the onset of RTN fluctuations followed by a saturation at longer times. Note that, contrary to data in Fig. 5b, the analytical model predicts a smooth broadening with time, which corresponds to averaging all possible onset times of RTN. A numerical simulation of RTN was performed, resulting in the time-domain evolution in Fig. 5c, and the relative standard deviation σ_I/I

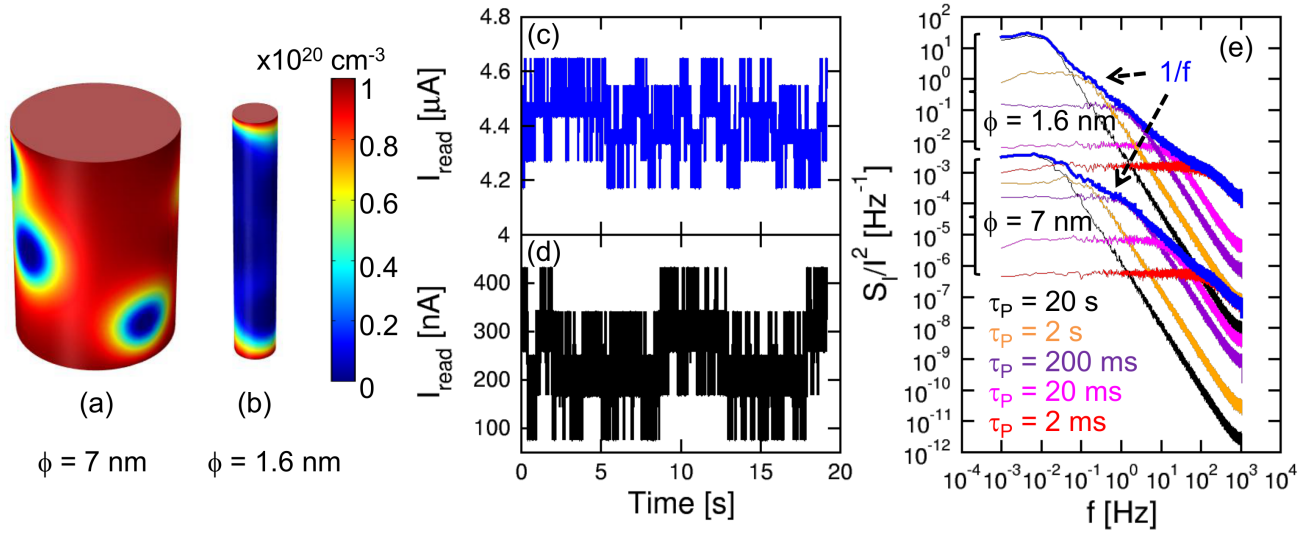

Fig. 9. Calculated carrier density at the CF surface in presence of 5 bistable fluctuating defects for diameters ϕ = 7 nm (a) and 1.6 nm (b), calculated I_{read} for ϕ = 7 nm (c) and 1.6 nm (d), and calculated S_I/I^2 (e). Note that the $1/f$ slope originates from the envelope of individual RTN components with different characteristic times τ_P.

in Fig. 5d. The analytical calculation is also reported here for comparison, confirming the validity of our analytical model. Finally, Fig. 5e shows the measured PSD and calculations from the numerical model and the analytical model of Eq. (4). Note the Lorentzian shape of the PSD which accounts for the saturating broadening at long times in Fig. 5b and d.

V. Resistance Dependence of Noise

The analytical model allows to predict the resistance distribution broadening based on parameter A, namely the PSD at 1 Hz for $1/f$ noise in Eq. (2). To assess the resistance dependence of broadening, we studied the PSD for different programmed HRS and LRS. Current noise was measured in a range of resistance of more than 3 decades from about 3 kΩ to about 5 MΩ. Fig. 6 shows the measured I_{read} as a function of time (a) and the corresponding S_I/I^2 (b) for increasing initial resistances, namely R_1 = 10 kΩ R_2 = 40 kΩ, R_3 = 320 kΩ and R_4 = 2.6 MΩ. All data show a $1/f$ spectrum of noise (RTN was found only in a minority of cases), where S_I/I^2 increases for increasing resistance, then saturates for HRS with relatively large resistance. To confirm the results in Fig. 6, data were collected for several samples, each programmed in various HRS and LRS, and S_I/I^2 was evaluated. Fig. 7 shows the resulting S_I/I^2 measured at 1 Hz as a function of the resistance. Two different stacks A and B were measured, differing for the metal oxide in the switching layer although no differences arise from the two different materials. Data show an increase of noise with resistance for R < 80 kΩ, followed by a saturation for R > 80 kΩ. Note the relatively large spread in the values of S_I/I^2 reported in the figure at any given R.

To support the role of $1/f$ noise in the broadening of the resistance distribution, Fig. 8 shows the scatter plot which correlates the measured relative spread σ_I/I taken at 520 s and the corresponding S_I/I^2 taken at 1 Hz. All data in the figure indicate a slope 0.5 on the loglog plot, which corresponds to a power law $\sigma_I/I \propto \sqrt{S_I/I^2}$. This power law can be understood by the relationship between $1/f$ PSD and the time-dependent broadening in Eq. (2). In fact, S_I at 1 Hz corresponds to parameter A in Eq. (2) for $1/f$ noise, thus accounting for the slope 0.5 in Fig. 8 according to Eq. (2) where $\sigma_I/I \propto \sqrt{S_I/I^2}$. The calculated line from Eq. (2) is also shown in the figure, which further supports the validity of Eq. (2) at variable resistance levels. Data from 2 RRAM devices with different stacks, namely stack A and B, are compared in Figs. 7 and 8: the 2 stacks show similar behavior, suggesting that noise and broadening cannot be easily suppressed by changing the oxide composition in the switching layer. Due to the large statistical spread in Figs. 7 and 8, it is not possible to rule out a minor difference due to the different oxide stacks A and B [24]. Previously, it was shown that the set operation with the same compliance current and different oxides resulted in different CF size [24], [25]. On the other hand, our previous works have shown that the relative noise amplitude of RTN only depends on R [11], therefore different CF sizes still result in the same 'universal' noise-resistance characteristics of Figs. 7 and 8. This explains the independence of noise characteristics on the details of the RRAM stack in our data.

The two regimes in Fig. 7 can be explained by the size dependence of noise as in the RTN case [11], [13]. Here, bistable defects, namely charged/uncharged point defects such as oxygen vacancies [26], [27] or Cu impurities [28], close to the CF surface in LRS fluctuate between two different charge states, hence resulting in an intermittent depletion of carriers within the CF. As R increases, the CF becomes smaller, thus resulting in a transition from partial depletion at low R to full depletion at large R [11]. For HRS, a similar explanation applies, except that the CF is replaced by a percolation conductive path with PF conduction. To provide a quantitative explanation of size dependent noise in Figs. 6 and 7, we calculated $1/f$ noise as the superposition of

several RTN contributions [11]. Noise was thus simulated in the time and frequency domain by a numerical calculation performed with a 3D numerical model for RTN noise [11]. In the calculations, we assumed that 5 bistable defects were located in random position near the surface of each CF. Fig. 9 shows the contour map of the carrier concentration at the CF surface for a relatively large CF with diameter ϕ = 7 nm (a) and a relatively small CF with ϕ = 1.6 nm (b), assuming that all 5 defects are in a negatively-charged state, thus resulting in a local depletion of carriers. In the figure, depleted regions with low carrier concentration can be recognized by the blue color. For the thick CF in Fig. 9a, only a limited portion of the CF cross-section is depleted, while the thin CF in Fig. 9b is fully depleted due to the CF diameter being smaller than the Debye length for carrier screening. To calculate the noise current as a function of time, we assumed independent, random switching of each bistable defect between a negative and a neutral state. Defects were assumed to have different characteristic times τ_P = 2 ms, 20 ms, 200 ms, 2 s, 20 s. Individual times τ_{on} and τ_{off} in Eq. (3) where assumed equal (τ_{on} = τ_{off} = $2\tau_P$) for each defect. We adopted equal time constants τ_{on} = τ_{off} for the sake of generality. However, similar results could be obtained with different τ_{on}/τ_{off} ratio, corresponding to different stability for neutral and charged states. All defects were assumed to be located at the surface of the CF, which resulted in the fluctuation amplitude ΔI being approximately the same for all defects. The calculated current measured at V_{read} = 50 mV as a function of time is reported in Fig. 9 for ϕ = 7 nm (c) and 1.6 nm (d). The CFs display resistance values of 11 kΩ (ϕ = 7 nm) and 200 kΩ (ϕ = 1.6 nm). Note that the bistable switching of the 5 defects results in 2^5 different current levels in the fluctuations, where each level is barely recognizable. Fig. 9e shows the S_I/I^2 of the calculated currents in Figs. 9c and d: S_I/I^2 is larger for the thinner CF than for the thicker CF, which is consistent with the experimental findings of Fig. 7 and is due to the size-dependent depletion in Fig. 9a and b. Fig. 9e also shows the S_I/I^2 of the RTN contributions due to the individual bistable fluctuations, revealing the typical Lorentzian behavior with a $1/f^2$ trend. By summing all RTN contributions one gets the overall $1/f$ distribution of noise power, which is consistent with data in Figs. 2 and 6. The $1/f$ fluctuation of current in our device can thus be interpreted as the superposition of several individual defects switching at distributed characteristic times.

VI. Acknowledgment

The authors thank Zhong-Qiang Wang for help with the experimental analysis of RRAM devices.

VII. Conclusions

This work addresses low-frequency noise in resistive switching devices by a detailed study of the 2 main contributions to current fluctuations, namely $1/f$ noise and RTN. We show that the broadening of the distributions of current and resistance can be predicted by an analytical model for the relationship between distribution broadening and noise PSD. Analytical models for $1/f$ noise and RTN are presented and confirmed by data and numerical Monte Carlo simulations of noise. Finally we studied the resistance dependence of the noise spectral density and broadening providing evidence for 2 different regimes at relatively low and high resistance, corresponding to partial and complete depletion of carriers in the CF by the fluctuating defect. A numerical finite-element model for noise with multiple fluctuation defects has been used in support of our interpretation.

References

[1] H.-S. P. Wong, H.-Y. Lee, S. Yu, Y.-S. Chen, Y. Wu, P.-S. Chen, B. Lee, F. T. Chen, and M.-J. Tsai, "Metal-oxide RRAM," *Proc. IEEE*, vol. 100, no. 6, pp. 1951–1970, 2012.

[2] M. Kozicki, C. Gopalan, M. Balakrishnan, and M. M. Mitkova, "A low-power nonvolatile switching element based on copper-tungsten oxide solid electrolyte," *IEEE Transactions on Nanotech.*, vol. 5, no. 5, pp. 535–544, 2006.

[3] I. Valov, R. Waser, J. Jameson, and M. Kozicki, "Electrochemical metallization memories–fundamentals, applications, prospects," *Nanotech.*, vol. 22, p. 254003, 2011.

[4] J. Jameson, P. Blanchard, C. Cheng, J. Dinh, A. Gallo, V. Gopalakrishnan, C. Gopalan, B. Guichet, S. Hsu, D. Kamalanathan, D. Kim, F. Koushan, M. Kwan, K. Law, D. Lewis, Y. Ma, V. McCaffrey, S. Park, S. Puthenthermadam, E. Runnion, J. Sanchez, J. Shields, K. Tsai, A. Tysdal, D. Wang, R. Williams, M. Kozicki, J. Wang, V. Gopinath, S. Hollmer, and M. V. Buskirk, "Conductive-bridge memory (CBRAM) with excellent high-temperature retention," *IEDM Tech Dig.*, pp. 30.1.1–30.1.4, 2013.

[5] H. Y. Lee, P. S. Chen, T. Y. Wu, Y. S. Chen, C. C. Wang, P. J. Tzeng, C. H. Lin, F. Chen, C. H. Lien, and M.-J. Tsai, "Low power and high speed bipolar switching with a thin reactive Ti buffer layer in robust HfO_2 based RRAM," *IEDM Tech. Dig.*, pp. 297–300, 2008.

[6] S. Ambrogio, S. Balatti, A. Cubeta, A. Calderoni, N. Ramaswamy, and D. Ielmini, "Statistical fluctuations in HfO_x resistive-switching memory (RRAM): Part I - Set/Reset variability," *IEEE Trans. Electron Devices*, vol. 61, no. 8, pp. 2912–2919, 2014.

[7] S. Ambrogio, S. Balatti, V. McCaffrey, D. Wang, and D. Ielmini, "Impact of low-frequency noise on read distributions of resistive switching memory (RRAM)," *IEDM Tech. Dig.*, pp. 1–4, 2014.

[8] S. Yu, R. Jeyasingh, Y. Wu, and H.-S. P. Wong, "Understanding the conduction and switching mechanism of metal oxide RRAM through low frequency noise and AC conductance measurement and analysis," *IEDM Tech. Dig.*, pp. 275–278, 2011.

[9] Z. Fang, H. Y. Yu, W. J. Fan, G. Ghibaudo, J. Buckley, B. DeSalvo, X. Li, X. P. Wang, G. Q. Lo, and D. L. Kwong, "Current conduction model for oxide-based resistive random access memory verified by low.frequency noise analysis," *IEEE Trans. Electron Devices*, vol. 60, no. 3, pp. 1272–1275, 2013.

[10] D. Veksler, G. Bersuker, L. Vandelli, A. Padovani, L. Larcher, A. Muraviev, B. Chakrabarti, E. Vogel, D. C. Gilmer, and P. D. Kirsch, "Random telegraph noise (RTN) in scaled RRAM devices," *International Reliability Physics Symposium (IRPS)*, pp. 101–104, 2013.

[11] S. Ambrogio, S. Balatti, A. Cubeta, A. Calderoni, N. Ramaswamy, and D. Ielmini, "Statistical fluctuations in HfO_x resistive-switching memory (RRAM): Part II - Random telegraph noise," *IEEE Trans. Electron Devices*, vol. 61, no. 8, pp. 2920–2927, 2014.

[12] N. Raghavan, R. Degraeve, A. Fantini, L. Goux, S. Strangio, B. Govoreanu, D. J. Wouters, G. Groeseneken, and M. Jurczak, "Microscopic origin of random telegraph noise fluctuations in aggressively scaled RRAM and its impact on read disturb variability," *International Reliability Physics Symposium (IRPS)*, pp. 5E.3.1–5E.3.7, 2013.

[13] D. Ielmini, F. Nardi, and C. Cagli, "Resistance-dependent amplitude of random telegraph-signal noise in resistive switching memories," *Appl. Phys. Lett.*, vol. 96, no. 5, p. 053503, 2010.

[14] D. Lee, J. Lee, M. Jo, J. Park, M. Siddik, and H. Hwang, "Noise-analysis-based model of filamentary switching ReRAM with ZrO_x/HfO_x stacks," *IEEE Electron Dev. Lett.*, vol. 32, no. 7, pp. 964–966, 2011.

[15] R. Soni, P. Meuffels, A. Petraru, M. Weides, C. Kugeler, R. Waser, and H. Kohlstedt, "Probing Cu doped $Ge_{0.3}Se_{0.7}$ based resistance switching memory devices with random telegraph noise," *J. Appl. Phys.*, vol. 107, no. 2, p. 024517, 2010.

[16] L. Gao, F. Alibart, and D. Strukov, "Analog-input analog-weight dot-product operation with Ag/a-Si/Pt memristive devices," *VLSI and System-on-Chip (VLSI-SoC) Tech. Dig.*, pp. 88–93, 2012.

[17] Y. Tseng, W. Shen, C.-E. Huang, C. Lin, and Y.-C. King, "Electron trapping effect on the switching behavior of contact RRAM devices through random telegraph noise analysis," *IEDM Tech. Dig.*, pp. 28.5.1–28.5.4, 2010.

[18] S. Ambrogio, S. Balatti, V. McCaffrey, D. Wang, and D. Ielmini, "Noise-induced resistance broadening in resistive switching memory (RRAM) - Part II: Array statistics," *IEEE Trans. Electron Devices*, vol. Submitted.

[19] M. Kund, G. Beitel, C.-U. Pinnow, T. Rohr, J. Schumann, R. Symanczyk, K.-D. Ufert, and G. Muller, "Conductive bridging RAM (CBRAM): an emerging non-volatile memory technology scalable to sub 20 nm," *IEDM Tech. Dig.*, pp. 754–757, 2005.

[20] S. Larentis, F. Nardi, S. Balatti, D. C. Gilmer, and D. Ielmini, "Resistive switching by voltage-driven ion migration in bipolar RRAM - Part II: Modeling," *IEEE Trans. Electron Devices*, vol. 59, no. 9, pp. 2468–2475, 2012.

[21] S. Ambrogio, S. Balatti, S. Choi, and D. Ielmini, "Impact of the mechanical stress on switching characteristics of electrochemical resistive memory," *Adv. Mat.*, vol. 26, no. 23, p. 3885, 2014.

[22] P. R. Gray, P. J. Hurst, S. H. Lewis, and R. G. Meyer, "Analysis and design of analog integrated circuits," *John Wiley & Sons, Inc.*, 2001.

[23] S. Machlup, "Noise in semiconductors: spectrum of a two-parameter random signal," *J. Appl. Phys.*, vol. 25, no. 3, pp. 341–343, 1954.

[24] L. Goux, A. Fantini, R. Degraeve, N. Raghavan, R. Nigon, S. Strangio, G. Kar, D. Wouters, Y. Chen, M. Komura, F. D. Stefano, V. Afanas'ev, and M. Jurczak, "Understanding of the intrinsic characteristics and memory trade-offs of sub-μA filamentary RRAM operation," *Symp. VLSI*, pp. T162–T163, 2013.

[25] D. Ielmini, "Modeling the universal set/reset characteristics of bipolar RRAM by field- and temperature-driven filament growth," *IEEE Trans. Electron Devices*, vol. 58, no. 12, pp. 4309–4317, 2011.

[26] J. L. Gavartin, D. M. Ramo, A. L. Shluger, G. Bersuker, and B. H. Lee, "Negative oxygen vacancies in HfO_2 as charge traps in high-k stacks," *Appl. Phys. Lett.*, vol. 89, p. 082908, 2006.

[27] A. L. Shluger and K. P. McKenna, "Models of oxygen vacancy defects involved in degradation of gate dielectrics," *IRPS Tech. Dig.*, p. 5A.1, 2013.

[28] A. Padilla, G. W. Burr, R. S. Shenoy, K. V. Raman, D. S. Bethune, R. M. Shelby, C. T. Rettner, J. Mohammad, K. Virwani, P. Narayanan, A. K. Deb, R. K. Pandey, M. Bajaj, K. V. R. M. Murali, B. N. Kurdi, , and K. Gopalakrishnan, "On the origin of steep I-V nonlinearity in Mixed-Ionic-Electronic-Conduction-Based Access Devices," *IEEE Trans. on Electron Dev.*, vol. 62, no. 3, pp. 963–971, 2015.